GA–A24281

QUANTITATIVE TESTS OF ELMs AS INTERMEDIATE n PEELING-BALLOONING MODES

by
L.L. LAO, P.B. SNYDER, A.W. LEONARD, T. OIKAWA, T.H. OSBORNE,
T.W. PETRIE, J.R. FERRON, R.J. GROEBNER, L.D. HORTON,
Y. KAMADA, M. MURAKAMI, S. SAARELMA, H.E. ST JOHN,
A.D. TURNBULL, and H.R. WILSON

MARCH 2003

DISCLAIMER

GA–A24281

QUANTITATIVE TESTS OF ELMs AS INTERMEDIATE n PEELING-BALLOONING MODES

by
L.L. LAO, P.B. SNYDER, A.W. LEONARD, T. OIKAWA,* T.H. OSBORNE, T.W. PETRIE, J.R. FERRON, R.J. GROEBNER, L.D. HORTON,† Y. KAMADA,* M. MURAKAMI,‡ S. SAARELMA,# H.E. ST JOHN, A.D. TURNBULL, and H.R. WILSON△

This is a preprint of a paper to be submitted for publication in *Plasma Physics and Controlled Fusion.*

*Japan Atomic Energy Research Institute, Japan.
†Max Planck Institute of Plasma Physics, Garching, Germany.
‡Oak Ridge National Laboratory, Oak Ridge, Tennessee.
#Helsinki University of Technology, Finland.
△EURATOM/UKAEA Fusion Association, Abingdon, United Kingdom.

Work supported by
the U.S. Department of Energy
under Contract Nos. DE-AC03-99ER54463, DE-AC05-00OR22725
and DE-FG03-95ER54309

GENERAL ATOMICS PROJECT 30033
MARCH 2003

ABSTRACT

Several testable features of the working model of edge localized modes (ELMs) as intermediate toroidal mode number peeling-ballooning modes are evaluated quantitatively using DIII-D and JT-60U experimental data and the ELITE MHD stability code. These include the hypothesis that ELM sizes are related to the radial widths of the unstable MHD modes, the unstable modes have a strong ballooning character localized in the outboard bad curvature region, and ELM size generally becomes smaller at high edge collisionality. ELMs are triggered when the growth rates of the unstable MHD modes become significantly large. These testable features are consistent with many ELM observations in DIII-D and JT-60U discharges.

I. INTRODUCTION

This paper describes recent quantitative tests of this model using experimental data from the DIII-D and the JT-60U tokamaks. These tests are made possible by recent improvements to the ELITE MHD stability code [3,5], which allow an efficient evaluation of the unstable peeling-ballooning modes, as well as by improvements to diagnostic and analysis techniques. Some of the key testable features of this model are:

1. ELMs are triggered when the growth rates of the unstable MHD modes become significantly large;

2. ELM sizes are related to the radial widths of the unstable modes;

3. The unstable modes have a strong ballooning character localized in the outboard bad curvature region;

4. At high collisionality, ELM size generally becomes smaller because J_{BS} is reduced.

These testable features are consistent with many ELM observations in DIII-D and JT-60U discharges. The predicted growth rate attains a significant value just before an ELM occurs and the observed change in electron temperature $\Delta T_e/T_e$, before and after an ELM, from statistical analysis of DIII-D Thomson data is consistent with the calculated radial width of the most unstable peeling-ballooning mode. The predictions of small or large radial widths of the unstable modes are also consistent with the small or giant ELMs observed in JT-60U. The absence of ELM-generated particle flux on the inboard side of DIII-D double-null divertor discharges supports the strong ballooning character of these modes. The reduction of ELM energy loss observed in DIII-D high density discharges from gas-puff experiments is consistent with the decrease of ELM size at high collisionality.

This paper is organized as follows. The peeling-ballooning working model of ELM is summarized in Section II. In Section III, tests of ELM triggering and its size against DIII-D and JT-60U data are discussed. Test of the ELM ballooning character is presented in Section IV. In Section V, test of the collisionality effect on ELM size is discussed. A summary is given in Section VI.

II. PEELING-BALLOONING WORKING MODEL OF ELM

Stability analyses and experimental results [1-4], particularly those from the DIII-D experiments varying the squareness parameter, suggest an ideal stability based working model of ELMs as intermediate *n* peeling-ballooning modes. In this model, the main driving forces for the instability are the edge P′ and J_{EDGE}, which interact through J_{BS} and its effects on stability. The ELM size is assumed to be related to the radial width of the unstable MHD modes. The critical edge P′ is set by the unstable modes with the highest *n* without the second ballooning stability access. This is schematically illustrated in Fig. 1.

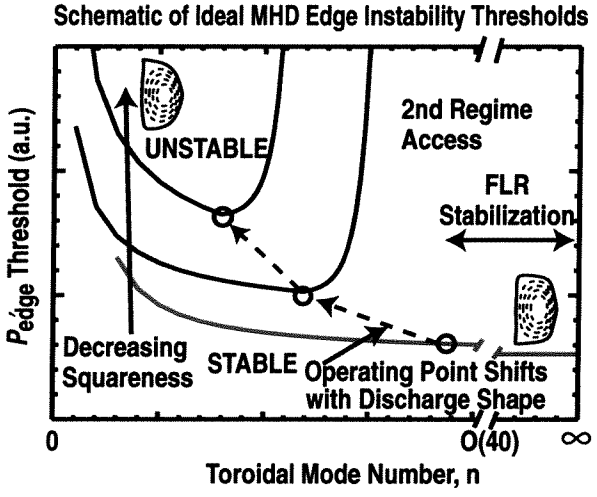

Fig. 1. A schematic drawing of the stability boundary in the edge pedestal region for three different discharge shapes with moderate to high squareness..

In this model, J_{EDGE} plays a dual role by stabilizing the high *n* ballooning modes and providing access to the second ballooning stability region, but providing free energy to drive the intermediate *n* peeling modes. As shown in Fig. 1, improving the plasma shape by reducing the squareness of the plasma boundary improves access to the second ballooning stability region. At high squareness, the edge region has no second stability access and the critical P′ is determined by the first ballooning stability limit not stabilized by the finite Larmor radius (FLR) effects. As squareness is reduced, the critical P′ is determined by the highest *n* mode without second ballooning stability access. These predictions are consistent with the experimental results from the DIII-D squareness

experiments [1,2]. Both the low-intermediate and the intermediate-high n branches of this diagram have been verified using the GATO and the ELITE stability codes [3,6].

III. ELM TRIGGERING AND SIZE

In this model, the ELM size is assumed related to the radial width of the unstable MHD modes. They are triggered when the growth rates of the unstable MHD modes become significantly large. These features are consistent with many experimental observations in DIII-D and JT-60U discharges. These are illustrated in Figs. 2 through 4. In Fig. 2, the calculated $n = 10$ normalized growth rates for a sequence of equilibria for a DIII-D VH-mode discharge at various times before the first large Type I ELM are shown. The growth rates are computed using the ELITE code based on experimental equilibria reconstructed from kinetic profiles and MSE data using the EFIT code [7]. The diamagnetic effects may contribute to the stabilization of the high n ballooning modes and improves the first ballooning stability limit [8-10]. These effects are not included in the ELITE calculations. They are roughly estimated by comparing the growth rates γ to $\omega^*/2$ [3]. Here, ω^* is the diamagnetic drift frequency. As shown in Fig. 2, the calculated growth rate attains a significant value just before an ELM occurs. Here the $n = 10$ mode is chosen for the comparison since it has the largest growth rate normalized to the diamagnetic frequency, γ/ω^*.

The observed change in electron temperature $\Delta T_e/T_e$ from statistical analysis of DIII-D Thomson data is consistent with the calculated radial width of the most unstable peeling-ballooning mode [3]. This is illustrated in Fig. 3, where the relative change in $\Delta T_e/T_e$ immediately after a giant ELM for a DIII-D discharge is compared against the radial width of the $n = 10$ unstable eigenmode. The change in $\Delta T_e/T_e$ is estimated by ordering the measured T_e profiles in time with respect to the ELMs over many ELM cycles and extrapolating the results to the time immediately after an ELM crash. Also

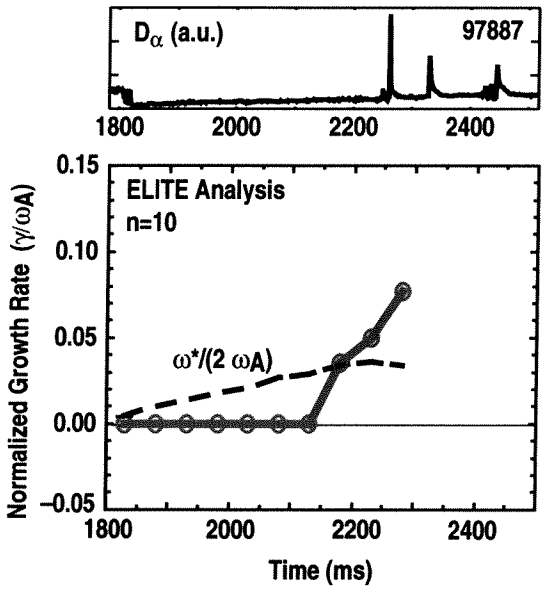

Fig. 2. Amplitude of the divertor D_α radiation signal is shown above, indicating the L-H transition and ELM times. Calculated n = 10 normalized growth rate as a function of time is shown below, along with an estimate of the normalized $\omega^*/2$ to describe the diamagnetic stabilization effects. The growth rates are normalized to the Alfven frequency ω_A.

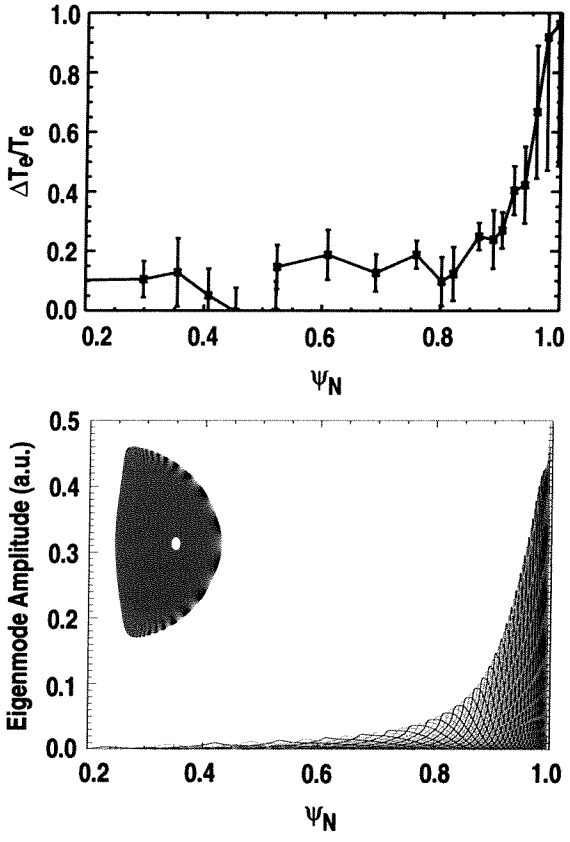

Fig. 3. Comparison of the radial profile of $\Delta T_e/T_e$ right after a giant ELM for DIII-D discharge 97887 against the radial structure of the unstable n = 10 peeling-ballooning mode computed using ELITE. A contour plot of the radial displacement of the unstable mode is shown in the inset.

shown in the inset of Fig. 3 is the 2-D contour of the MHD radial displacement. The perturbations are strongly pressure-driven and have a dominant ballooning character localized in the outboard bad curvature region. This is further discussed in Sec. IV.

The predicted radial widths of the unstable peeling-ballooning modes are also consistent with the JT-60U giant and grassy ELM experimental results [6,11]. The predicted unstable modes in the JT-60U grassy ELM discharges using ELITE based on experimental equilibria have narrower radial widths than those with large Type I ELMs [6]. This is illustrated in Fig. 4, where the radial structure of the unstable MHD modes for a JT-60U grassy ELM discharge and a discharge with large Type I ELMs are compared.

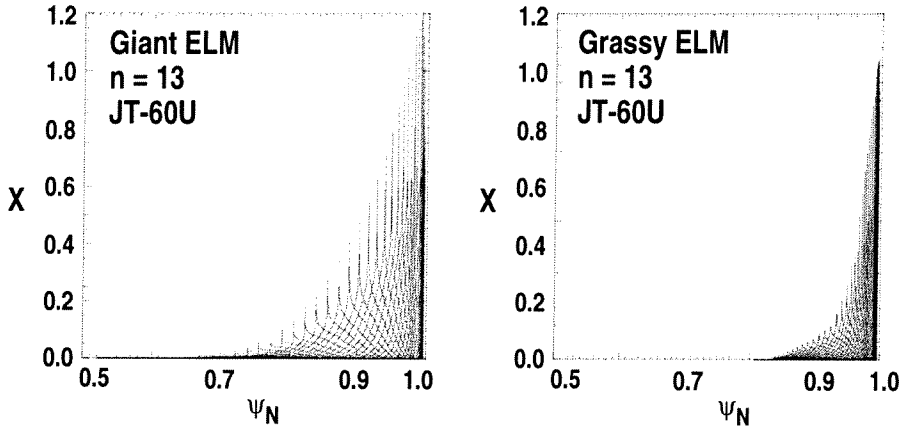

Fig. 4. Comparison of the radial structure of the unstable MHD modes computed using the ELITE edge stability code for a JT-60U discharge with large Type I ELM and one with small grassy ELM. ψ_N is the normalized poloidal flux.

IV. ELM BALLOONING CHARACTER

The unstable MHD modes are driven by the large edge pedestal P′ and the associated edge J_{BS}. Bad curvature plays a strong role in the instability. Thus, the predicted poloidal structure of the unstable eigen modes have a strong ballooning character localized in the outboard bad curvature region, as illustrated in the inset of Fig. 3. This predicted feature is consistent with the experimental results from the DIII-D divertor balance experiments [12]. ELM-generated particle fluxes to the inner strike point are observed in both lower-single-null and upper-single-null divertor discharges, but are absent in the double-null discharge when it is topologically disconnected from the outer mid-plane. This is illustrated in Fig. 5, where the particle fluxes at various poloidal locations around the divertor from Langmuir probe measurements for a lower-single-null discharge, a double-null discharge, and an upper-single-null discharge [Fig. 5(a)] are compared. The 2-D contours of the radial displacements computed using ELITE, based on experimentally reconstructed equilibria from these three discharges, are shown in Fig. 5(b). The perturbations are localized in the outboard bad curvature regions due to the strong ballooning character, consistent with the measurements of the ELM-generated particle fluxes in these discharges [Fig. 5(c)]. The experimental equilibria used in these analyses are reconstructed from kinetic profiles and MSE data using the EFIT code [7].

This predicted ballooning character is also consistent with the Mirnov oscillations sometimes observed in DIII-D discharges prior to a giant Type I ELM. These magnetic oscillations rotate in the electron diamagnetic direction, which is consistent with localization of these modes in the plasma edge region [13]. The Mirnov oscillations have a strong ballooning character localized poloidally in the outboard bad curvature region. Localized reflectometer measurements at the outboard mid-plane indicate that the perturbations start in the high pedestal pressure gradient region and propagate outwards into the scrape-off layer [1].

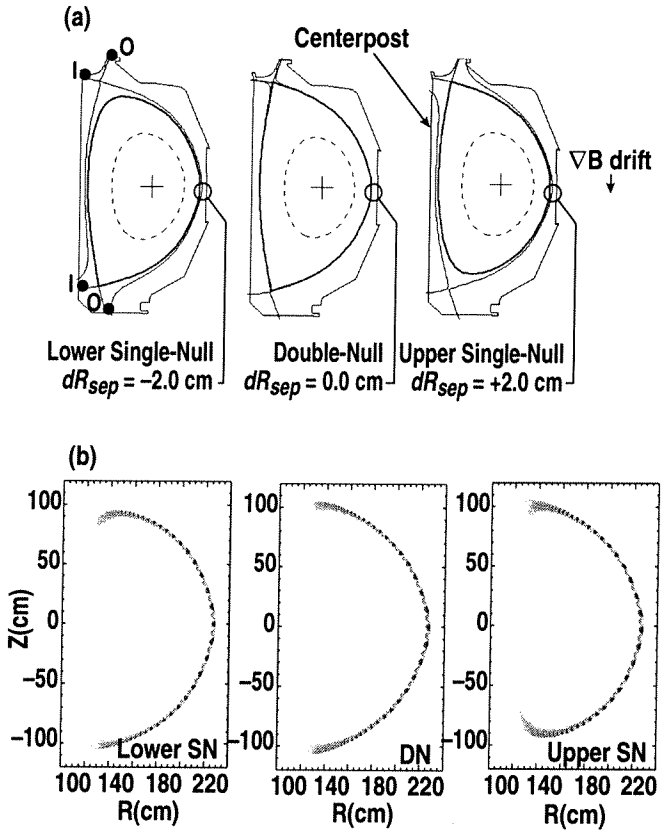

Fig. 5. (a) The lower-single-null, the double-null, and the upper-single-null divertor configurations used in the DIII-D divertor balance experiments. dR_{sep}, denotes the radial difference between the upper divertor separatrix flux surface and the lower divertor separatrix flux surface at the outer midplane. (b) Contours of the radial displacement of the unstable n = 25 peeling-ballooning modes showing the localization of the perturbations in the outboad bad curvature regions. (c) ELM-generated particle fluxes from Langmuir probes at various poloidal locations around the divertor showing the absence of ELM-generated particle flux in the double-null divertor discharge. (Page 1 of 2)

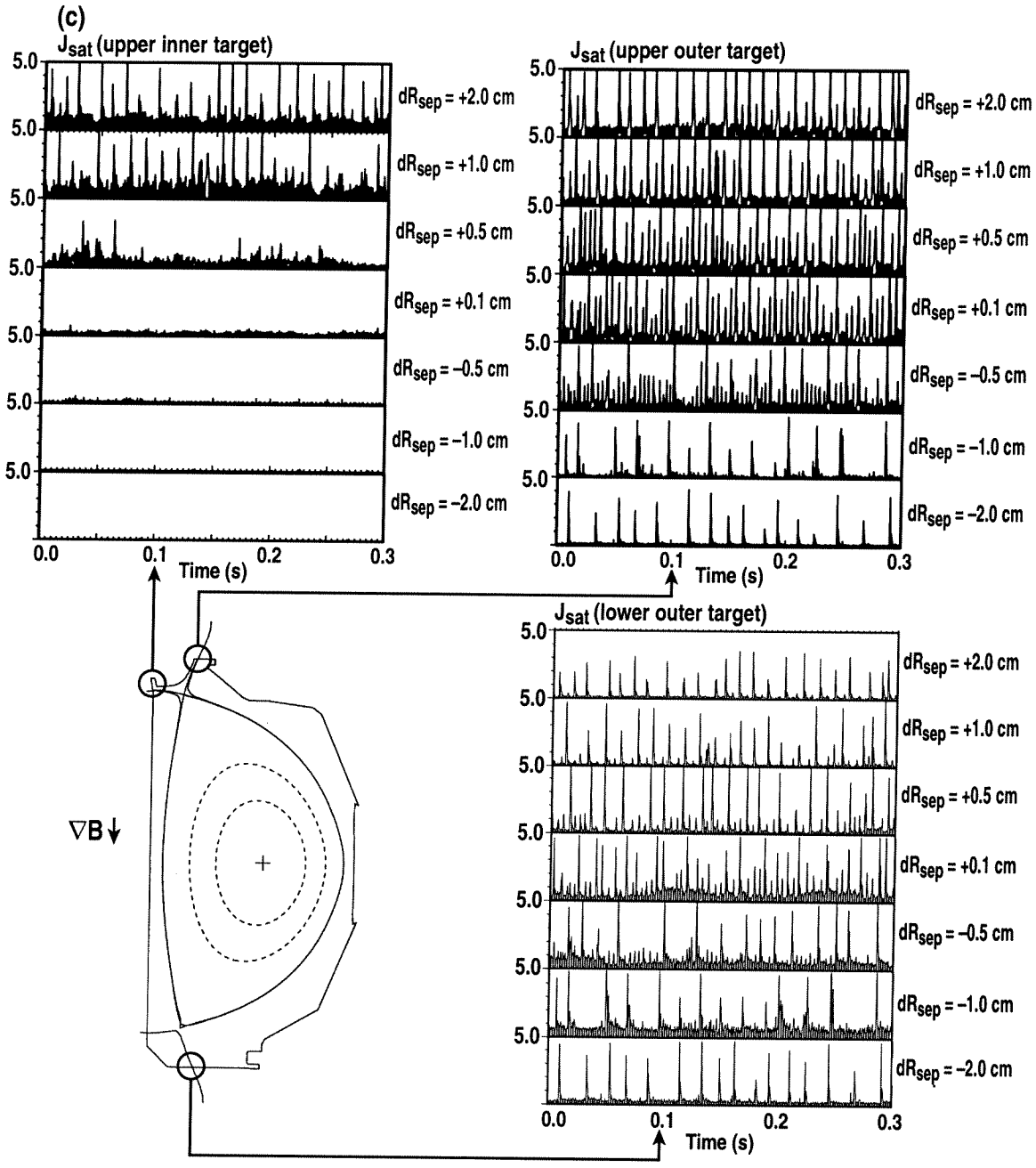

Fig. 5. (a) The lower-single-null, the double-null, and the upper-single-null divertor configurations used in the DIII-D divertor balance experiments. dR_{sep}, denotes the radial difference between the upper divertor separatrix flux surface and the lower divertor separatrix flux surface at the outer midplane. (b) Contours of the radial displacement of the unstable n = 25 peeling-ballooning modes showing the localization of the perturbations in the outboad bad curvature regions. (c) ELM-generated particle fluxes from Langmuir probes at various poloidal locations around the divertor showing the absence of ELM-generated particle flux in the double-null divertor discharge. (Page 2 of 2)

V. COLLISIONALITY

The MHD modes are driven by both the edge J_{BS} as well as the edge pedestal P′. As the edge density and hence the edge collisionality is increased, the ELM size is generally predicted to become smaller since J_{BS} is reduced. This is consistent with the experimental results from the DIII-D gas puff experiments. These are illustrated in Figs. 6 through 8. In Fig. 6, the ELM energy losses determined from equilibrium reconstructions using fast magnetic measurements for two DIII-D discharges with the edge Greenward density parameter $n_e/n_{GW} = 0.52$ and 0.74 are compared. The ELM energy loss is substantially reduced in the higher density discharge The relative change in the electron temperature before and after an ELM $\Delta T_e/T_e$ for these two discharges are compared in Fig. 7.

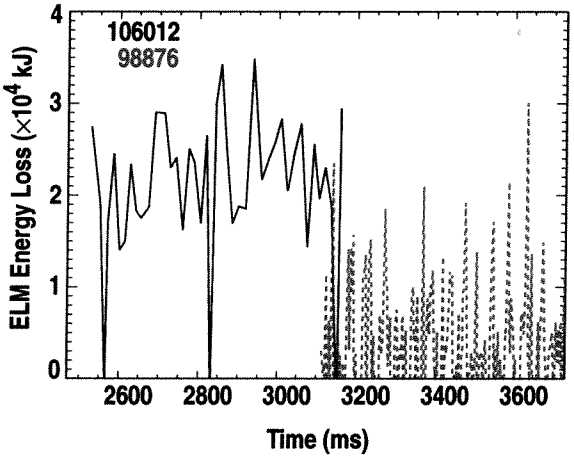

Fig. 6. Comparison of ELM energy loss for 2 DIII-D discharges with edge $n_e/n_{GW} = 0.52$ (solid curve) and $n_e/n_{GW} = 0.74$ (dashed curve).

The radial structures of the unstable eigenmodes computed using ELITE based on experimental equilibria reconstructed using kinetic profiles and MSE data are compared in Fig. 8. In these equilibria, J_{EDGE} is constrained using a bootstrap current model. As shown in Fig. 8, the unstable MHD mode for the smaller ELM, higher density discharge has a narrower radial width than the larger ELM, lower density discharge. The unstable mode in the higher density case has $n = 25$ and the lower density case has $n = 10$.

The increase in edge J_{BS} in the lower density case stabilizes the high n modes but destabilizes the lower n instabilities. This is illustrated in Fig. 9, where the high n ballooning stability diagrams for these two cases are compared. The lower density case

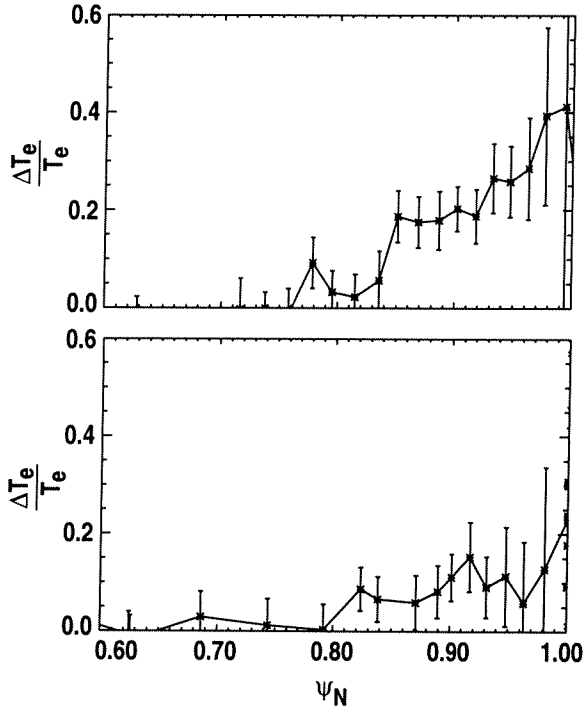

Fig. 7. Comparison of the radial profile of $\Delta T_e/T_e$ for the two DIII-D discharges shown in Fig. 6.

has second ballooning stability access in the plasma edge, whereas the higher density case does not. The edge second ballooning stability access in the lower density discharge is consistent with the wider edge pressure pedestal observed in this discharge.

This reduction of ELM size with collisionality since J_{BS} is reduced is also consistent with results from recent JT-60U current ramp experiments [14]. When J_{EDGE} is decreased by current ramp down during large Type I ELM phase, small grassy ELM state is obtained. Increasing J_{EDGE} by current ramp up during grassy ELM phase increases the ELM amplitude and change the ELM character to Type I.

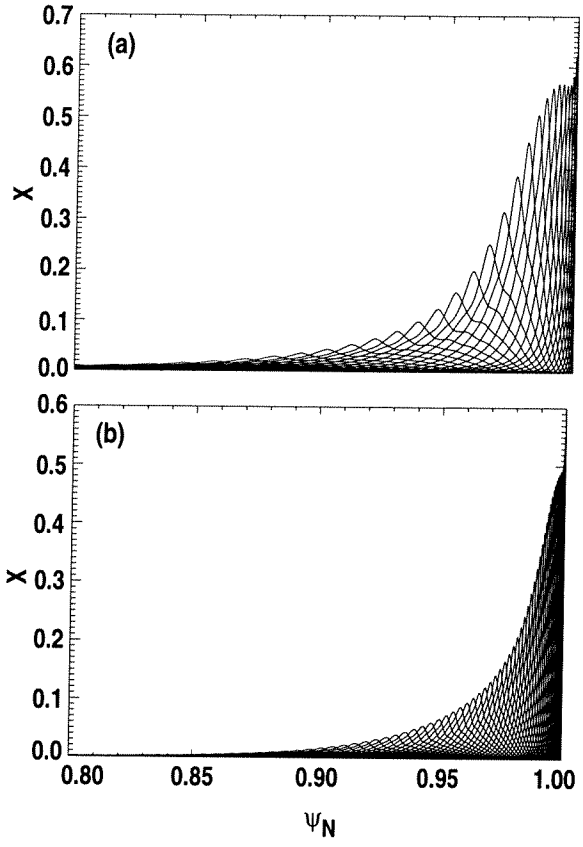

Fig. 8. Comparison of the radial structure of the unstable eigenmodes for the two DIII-D discharges shown in Fig. 6. (a) edge $n_e/n_{GW} = 0.52$ and $n = 10$ and (b) $n_e/n_{GW} = 0.74$ and $n = 25$. ψ_N is the normalized poloidal flux.

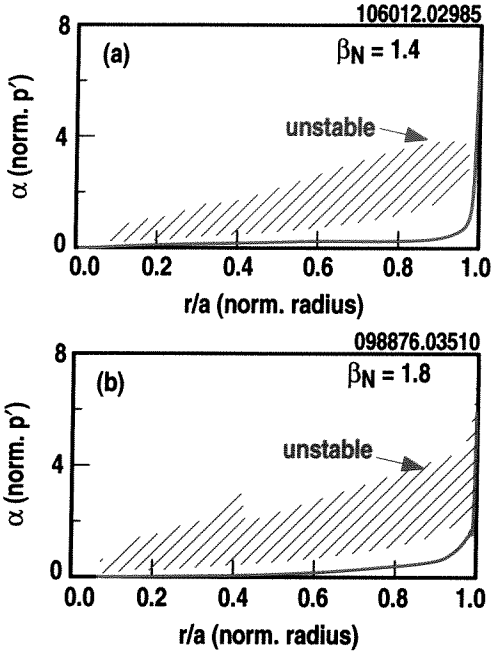

Fig. 9. Comparison of the high n ballooning stability boundary for the two DIII-D discharges shown in Fig. 6: (a) edge $n_e/n_{GW} = 0.52$ and (b) $n_e/n_{GW} = 0.74$.

VI. DISCUSSION AND SUMMARY

The key features of the working model of ELMs as intermediate $n \sim 5$–30 peeling-ballooning modes are consistent with many ELM observations in DIII-D and JT-60U discharges. ELMs are triggered when the growth rates of the intermediate n MHD modes become sufficiently large. The unstable modes have a strong ballooning character localized in the outboard bad curvature region. The ELM size is related to the radial width of the unstable MHD modes. As the edge collisionality is increased, ELM size is reduced since J_{BS} is decreased. Additionally, as previously reported [4,6,15], the increase of edge P' with the triangularity of the plasma shape observed in various tokamaks is also consistent with the prediction of this pelling-ballooning ELM model.

Although more work needs to be done to further test and improve this peeling-ballooning ELM model, these theorectical and experimental results provide strong support for this ELM model. It will be very interesting and illuminating to further test this ELM model against the ASDEX-U small type II ELM results [16] and the DIII-D QH-mode results [17]. Some of the issues and needs for this ELM model are: (1) magnetic precursors are not always observed, better detection and interpretaion techniques are needed; (2) more accurate J_{EDGE} measurements are needed to support the equilibrium reconstruction and stability analyses; (3) more fluctuation measurements are needed; (4) the effects of E×B flow shear on the MHD modes need to be investigated; and (4) nonlinear physics need to be included.

REFERENCES

[1] Lao, L.L., Ferron, J.R., Miller, R.L., *et al.*, (1999) *Nucl. Fusion* **39**, 1785.
[2] Ferron, J.R., Chu, M.S., Jackson, G.L., Lao, L.L., *et al.*, (2000) *Phys. Plasmas* **7**, (2000).
[3] Snyder, P.B., Wilson, H.R., Ferron, J.R., Lao, L.L., *et al.*, (2002) *Phys. Fluids* **9**, 2037.
[4] Saarelma, S., *et al.*, (2000) *Plasma Phys. Control. Fusion* **42**, A139.
[5] Wilson, H.R., Snyder, P.B., *et al.*, (2002) *Phys. Fluids* **9**, 1277.
[6] Lao, L.L., Kamada, Y., Oikawa, T., *et al.*, (2001) *Nucl. Fusion* **41**, 295.
[7] Lao, L.L., *et al.*, (1990) *Nucl. Fusion* **30**, 1035.
[8] Hahm, T.S. and Diamond, P.H., (1987) *Phys. Fluids* **30**, 133.
[9] Roger, B.N., *et al.*, (1999) *Phys. Plasmas* **6**, 2797.
[10] Hastie, R.J., *et al.*, (2000) *Phys. Plasmas* **7**, 4561.
[11] Kamada, S., *et al.*, (2000) *Plasma Phys. Control. Fusion* **42**, A247.
[12] Petrie, T.W., *et al.*, (2002) General Atomic Report GA-A23895.
[13] Strait, E.J., *et al.*, (1997) *Phys. Plasmas* **4**, 1783.
[14] Oikawa, T., *et al.*, (2002) *Bull. Am. Phys. Soc.* **47**, 270.
[15] Lao, L.L., (2000) *Plasma Phys. Control. Fusion* **42**, A51.
[16] Stober, J., *et al.*, (2001) *Nucl. Fusion* **41**, 1123.
[17] Burrell, K.H., *et al.*, (2002) *Plasma Phys. Control. Fusion* **44**, A253.

ACKNOWLEDGMENT

This is a report of work supported by the U.S. Department of Energy under Contract Nos. DE-AC03-99ER54463, DE-AC05-00OR22725, and Grant DE-FG03-95ER54309.